Flow and Loss Mechanisms in Volutes of Centrifugal Pumps

R.A. Van den Braembussche
von Kàrmàn Institute for Fluid Dynamics
72, Chaussée de Waterloo
1640 Rhode-Saint-Genèse
BELGIUM

vdb@vki.ac.be

ABSTRACT

These lecture notes provide an overview of the different inlet and outlet volutes for radial impellers. It describes the advantages and disadvantages of the different geometries, the relation between flow and geometry, the impact on the downstream or upstream impeller, the loss mechanisms and some loss prediction models. The main purpose is to provide an insight into the flow structure that can be used later to improve the performance or remediate some problems. The use of CFD is not discussed but the flow models presented here may help to get a better understanding of the CFD output.

INTRODUCTION

The main consequence of a non-axisymmetric inlet- or outlet volute is a spanwise and circumferential distortion of the flow (pressure, velocity and flow angles) at the inlet and outlet of the impeller. Inlet distortion causes incorrect incidence and circumferentially varying non-optimum flow patterns in the different impeller channels. This results in increased losses, unsteady blade loading and increased NPSH. Outlet distortions also create the circumferential variations of the impeller flow, induce varying blade loading and increase the radial load on the bearings. Both result in extra losses, blade vibration, noise, increased radial forces on the shaft, reduced operating range and increased risk of cavitation.

The interaction between the rotating impeller and the fixed inlet and/or outlet volutes results in an unsteady flow in the impeller and exit volute. An accurate prediction of the flow and losses requires a simultaneous prediction of the flow in all components by means of a 3D unsteady flow solver. This is a computationally expensive and time consuming calculation providing detailed flow characteristics in a huge number of points. An efficient use of those results requires an understanding of the flow and loss mechanisms and of their mutual interference.

Following provides a short overview of the main flow phenomena and loss mechanisms respectively for inlet and outlet volutes of centrifugal impellers. The reason of this separate discussion is the fundamental difference between the flow in both geometries. The interaction with the impeller is not investigated.

Symbols
  P   pressure
  R   radius from rotational centre
  r   radius from the volute centre

subscripts
  1   impeller inlet
  2   impeller exit, volute inlet

  3   volute outlet
  4   volute exit cone outlet
  R   radial
  S   swirl component
  T   through flow component

superscripts
  o   total flow conditions

1. INLET VOLUTES

1.1 Overall Comparison

Inlet volutes can take a large variety of different shapes. The simplest ones are curved channels of circular cross section, connecting the inlet pipe to the impeller inlet section. They differ by the streamwise variation of the cross section area and curvature radius of the central line. The impact of a streamwise cross section area variation on impeller inlet velocity distortion is quite substantial as shown on Fig. 1 [1]. The constant cross section inlet shows a velocity variation between .6 to 1.15 $\overline{W}_m$ and a 15.$^{\circ}$ variation of the flow angle. The acceleration of the flow on the convex side, followed by a deceleration toward the impeller inlet, is at the origin of a flow separation and large velocity deficit on the inner wall.


| a | b | c |
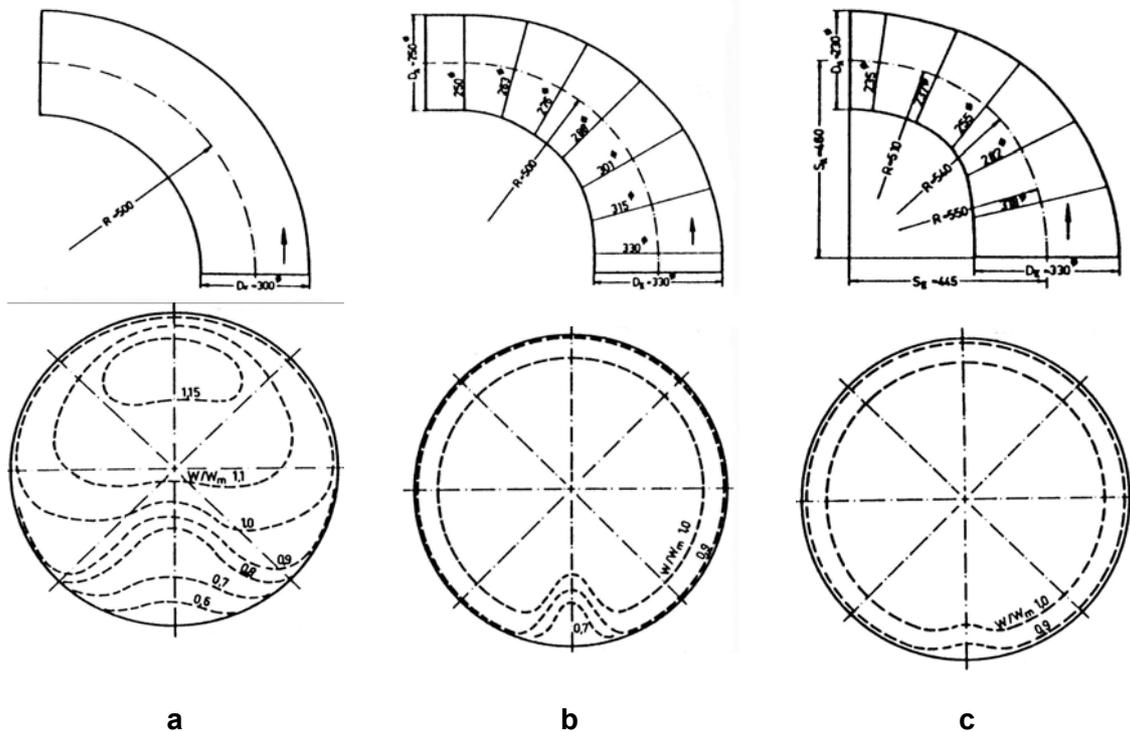
Figure 1: Different Types of Inlet Ducts and Corresponding Inlet Flow Distortion (Matthias [1]).

Depending on the convergence rate the non uniformity of the impeller inlet velocity is drastically reduced (Fig 1b) or has almost disappeared (Fig. 1c). Increasing the central line curvature radius is a second way to reduce this separation zone. However this is at the cost of a larger axial extend of the inlet. The design approach to obtain a more uniform inlet flow is by using the reduction of the cross section area to compensate for the local decelerations between the volute inlet and impeller leading edge on the inner part of the bend. The purpose is to obtain a velocity variation on the inner and outer wall of the tube as shown by the dashed line on Fig. 2. Inlet ducts of constant area show an acceleration of the flow on the convex side followed by a deceleration towards the impeller inlet. The later one is responsible for flow separation at the impeller inlet and can be avoided by a decrease of the cross section to keep the velocity constant up to the impeller inlet. The decrease of the cross section area limits the deceleration on the concave side and results in an increased acceleration towards the impeller inlet.
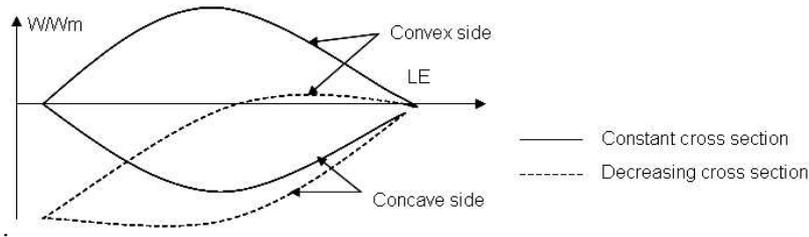
Figure 2: Influence of Convergence on the Inner and Outer Wall Velocity Distribution.

The uniformity of the flow can further be improved by optimizing the impeller nose to enhance the flow acceleration [2]. However a non symmetric nose as shown on Fig 3a can not rotate with the impeller and extra struts (and losses) are required to fix it.


a

b
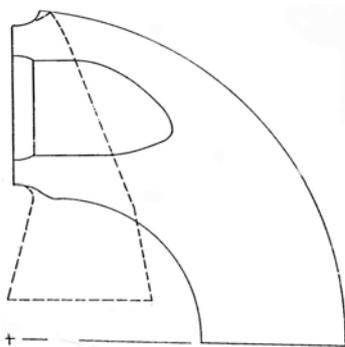
Figure 3a: Inlet Bend with Optimized Impeller Nose (_____) and Short Inlet Volute (_ _ _) (Pinckney [2]).
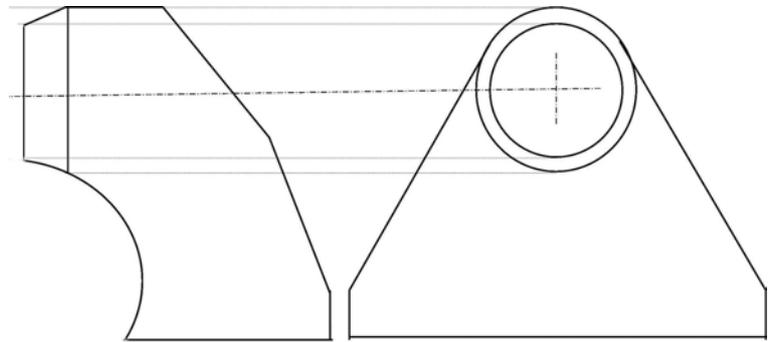
Figure 3b: Large Inlet Cavity.

The main disadvantage of curved inlet pipes is the long axial length and the large increase of losses and distortion generated by an eventual presence of a shaft at the inlet. An alternative for the curved tube is an inlet cavity (Fig. 3b) with deflection vanes or an inlet volute as shown on Fig 4a.
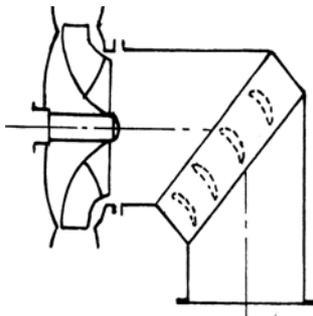
a
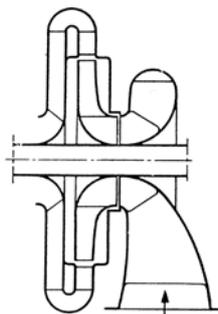
b
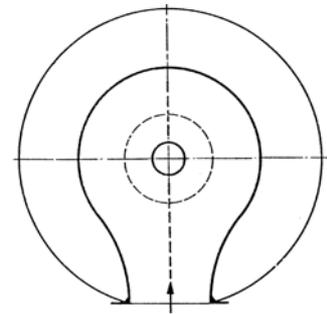
c

Figure 4: Cascade Bend (a) and Inlet Volute (b,c).

The inlet cascade (Fig. 4a) results in a quite uniform flow if the vanes are correctly placed. Pinckney [2] has analysed such a geometry and observed that large separation zones may occur near the convex side of

the bend. The later one was due to a flow separation upstream of the vanes and was remediated by putting the first vane further upstream at the concave side.

Table 1: Impact of Inlet Volute Geometry

	$\Delta H/(\rho.V^2/2)$	Δ NPSH (%)
Constant section bend (Fig. 1.a)	.04	30.
Convergent bend (Fig. 1.c)	.006	0.
Inlet cascade (Fig. 4.a)	.008	0.
Inlet volute with weak inlet convergence (Fig. 4c)	.030	0.12
Inlet volute with strong inlet convergence (Fig. 8)	.02	2.
Large inlet cavity (Fig. 3b)	.004	0.

Kovats [3] has estimated the impact of the different inlet geometries on losses and NPSH. His results are summarizeed in Table 1 and give an idea of the average head loss and increase in NPSH corresponding to the various inlet geometries. One observes increase of NPSH up to 30 %. One can also see that there exist geometries that have no measurable effect on head and NPSH (Fig. 3b). The main conclusion of this comparison is "converging ducts give much more even velocity distributions than ducts with constant flow area and the smaller the inner (convex side) radius is, the more distorted is the velocity profile".

1.2 Detailed Flow Studies

Lüdtke [4] made a detailed study of the flow in radial and tangential inlet volutes. The flow approaches the shaft at 180.$^{\text{o}}$ (Fig. 5a). The first location where the flow risks to separate is near the inlet upstream of the central core where the inlet duct diverges. A seconds one is on the convex side of the inlet bend where the flow turns from radial to axial for reasons already explained for curved inlet ducts. The third zone of flow separation is behind the shaft.

a   b
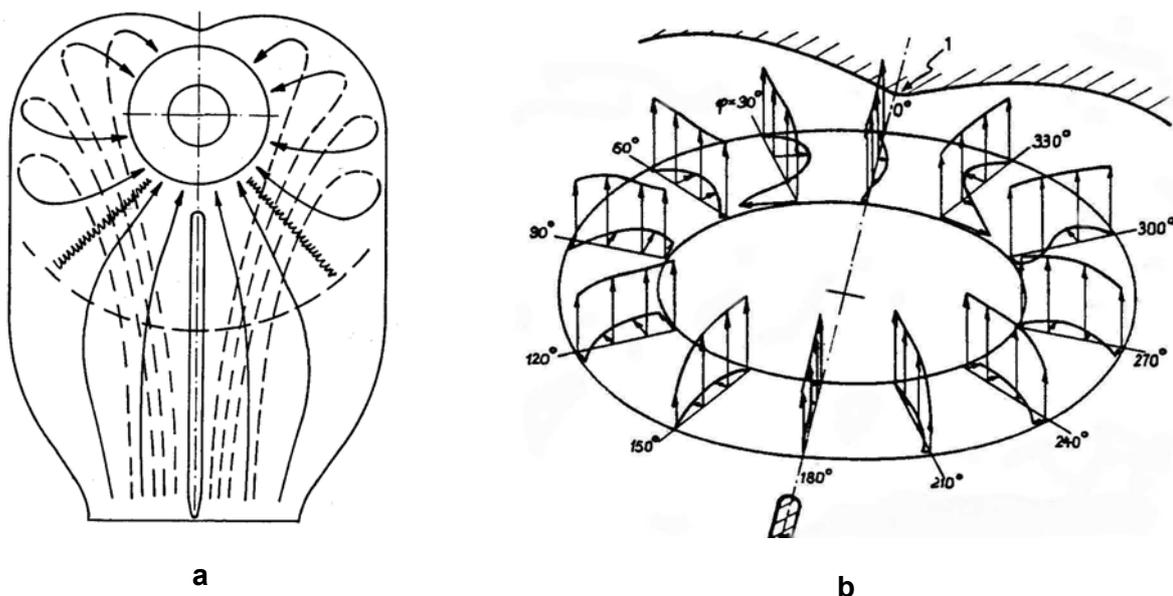
Figure 5: Flow Structure in a Radial Inlet Volute.

The streamlines at the top of the model (full lines on Fig. 5a) turn from radial to axial. The deceleration, because of the widening of the duct, is compensated by the local acceleration around the convex inlet shroud. This combination results in a quite uniform velocity (without separation) and zero swirl at the impeller inlet (180.$^{\circ}$ on Fig. 5b). The bottom streamlines (dashed lines) surround the shaft and flows backwards to feed the separated zone at the top on both sides of the diverging inlet duct. The rest of the flow turns around the shaft and fills the bottom part between 60.$^{\circ}$ and 300.$^{\circ}$ azimuth. This creates two counter rotating vortices at 30.$^{\circ}$ and 330.$^{\circ}$ when filling the separated flow zone downstream of the shaft.

Uniformity of the flow is improved when the eye is equipped with a bellmouth, to prevent the flow from entering the annulus in a non-axial way (Fig. 6). The concept of the bellmouth goes back to Stepanoff. has a double purpose. One is to avoid that the flow enters directly into the impeller near the inlet. The second one is to favour a more tangential approach of the shaft so that the flow will see a more elliptic cross section resulting in a reduced separation zone behind the shaft.
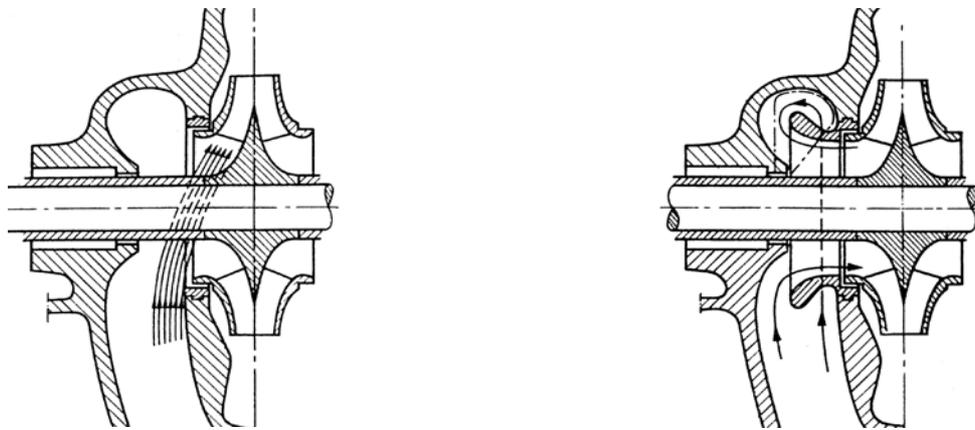

Figure 6: Impact of the Bellmouth on the Impeller Inlet Flow.

1.3   Tangential Inlet Volute

Tangential inlet ducts (Fig. 7) have a more uniform inlet velocity profile in axial and circumferential direction but a larger amount of swirl. However the increased swirl goes with a more uniform flow with smaller vortices [5] (Fig. 8).
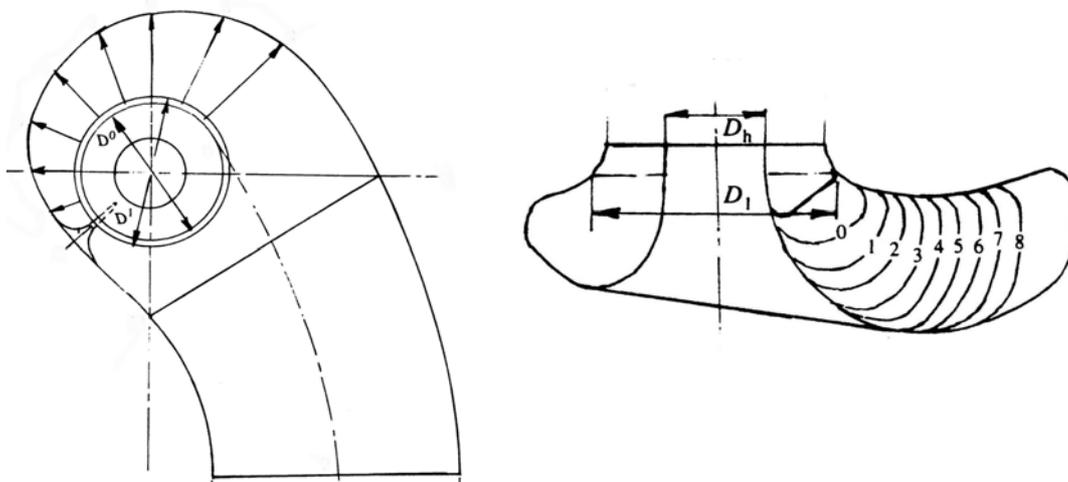

Figure 7: Tangential Inlet Volute.
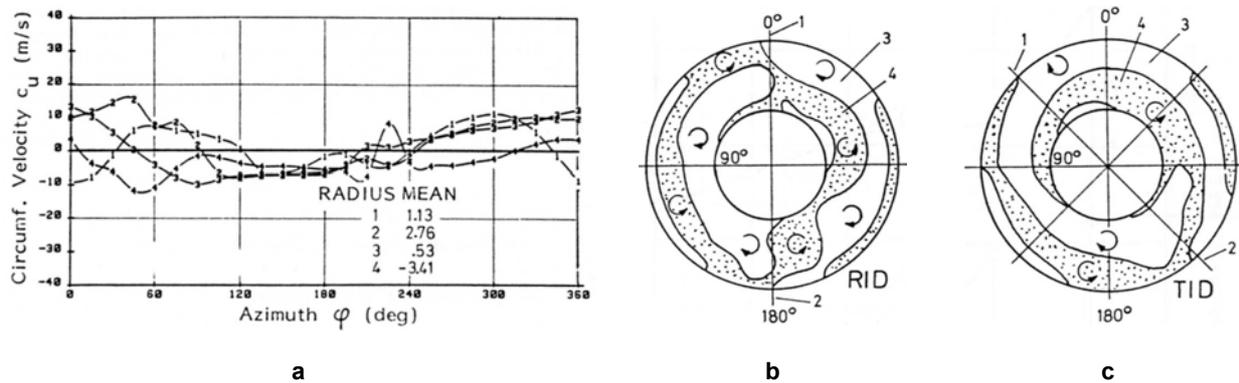
**Figure 8: Inlet Swirl Distribution in a Tangential Inlet Volute
(a) and Vorticity in a Radial (b) and Tangential (c) Volute.**

This kind of volute consists of:

- A transition piece, from a circular pipe to a quasi rectangular section. Flow uniformity is enhanced by introducing a small acceleration.

- The inlet volute, following a spiral tangent to the shroud of the inlet annulus. It can be subdivided in two zones. The first one is located at the convex side of the turn where the fluid approaches the annulus radially. The second one has a quasi-spiral form and is located at the outside of the turn, feeding the top of the annulus. The cross section changes gradually to compensate for the decrease in mass flow. The purpose is to keep the stagnation pressure and tangential velocity constant at the impeller eye similar to what is done with exit volutes. A second way to optimize the flow is by modifying the upstream splitter.

- A contracting section just upstream of the impeller eye (15 to 20%) to equalize the velocity distribution.

1.4   Impact of Inlet Geometry

Ligrani et al. [6] have made detailed studies of the losses and flow angle distributions for different inlet geometries. The total- and static pressure drop, dynamic pressure and flow angle are measured over the full circumference at five radii to assess the quality of the inlet. The basic geometry is shown in Fig. 9.
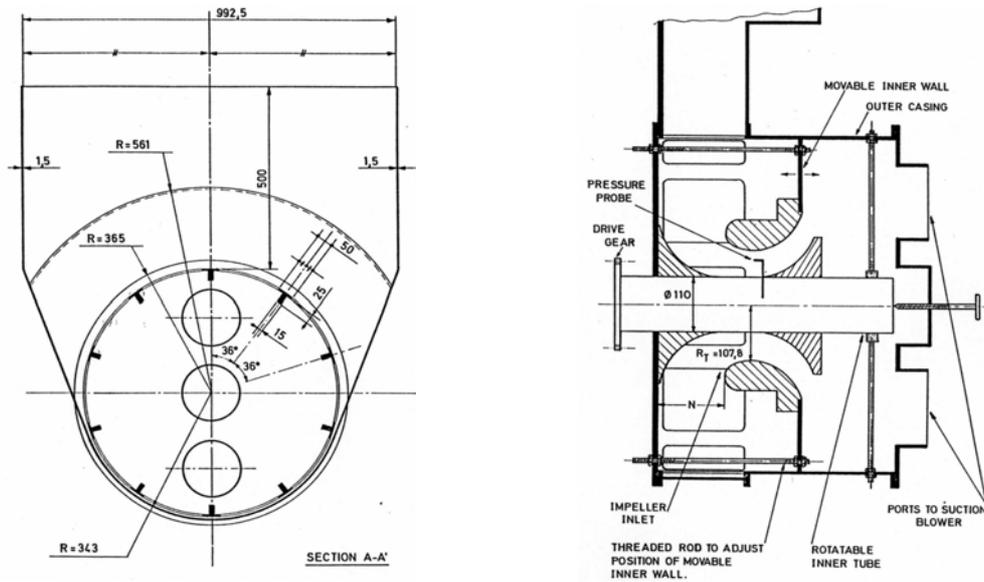
Figure 9: Basic Geometry.

Five struts of 50.mm width are located at radius 365.mm. The flow is sucked in a rectangular cross section duct by three orifices located behind the impeller exit. The influence of different ratios of inlet width to leading edge diameter (N/D = 0.741 (A), 0.531 (B), 0.351 (C) and 0.116 (D), N/D defined in Fig. 9) has been studied. The flow angle variation and total pressure loss coefficient are plotted on Fig.10 for geometry A. One observes large losses over the whole inlet plane with local extremes at 0 and +/- 60.° with respect to the top dead centre. The flow angle (Fig. 10b) shows an quasi-symmetric flow pattern with again the largest distortion and strong vortices at +/- 60.°.

a   b
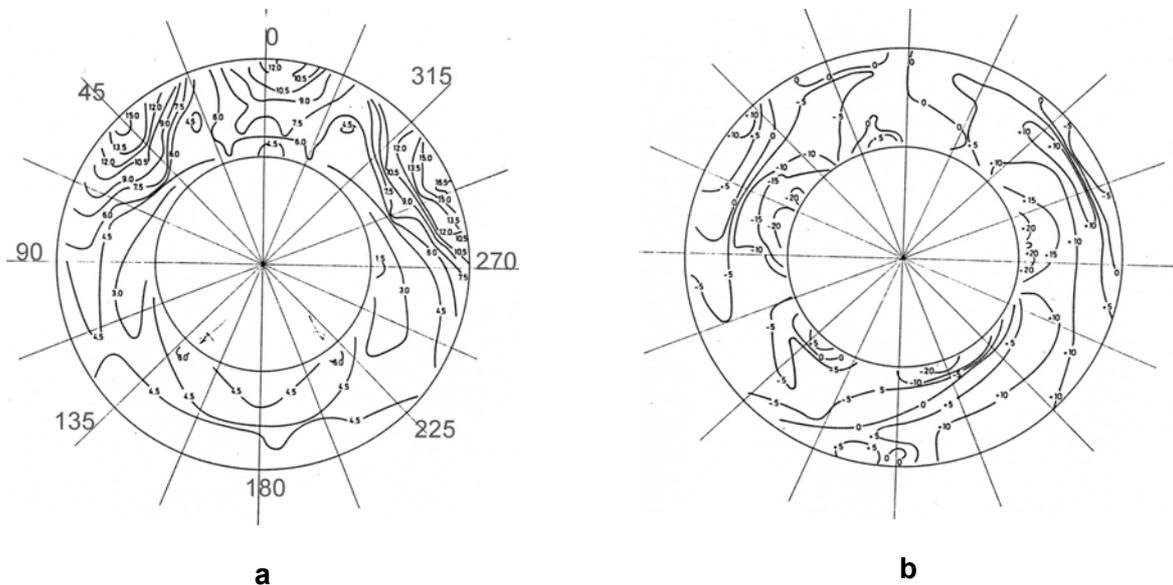
Figure 10: Absolute Flow Angle and Total Pressure Loss Variation at Impeller Inlet (N/D = .74).

The radial variation of the circumferentially averaged pressure loss is shown in Fig. 11a. Decreasing N/D to .535, decreases the losses and flow angle gradients. Plotting the average loss as a function of N/D

reveals the existence of a minimum as shown in Fig. 11b. This corresponds to the idea that diffusion plays a key role in the performance (losses and flow uniformity). Decreasing N/D increases the acceleration in the first part of the nozzle (inlet to bellmouth) but decreases it in the second part. As the disturbing elements (struts) are located in the first part of the nozzle, the flow is more sensitive to diffusion in this part.

<div align="center">a</div>

<div align="center">b</div>
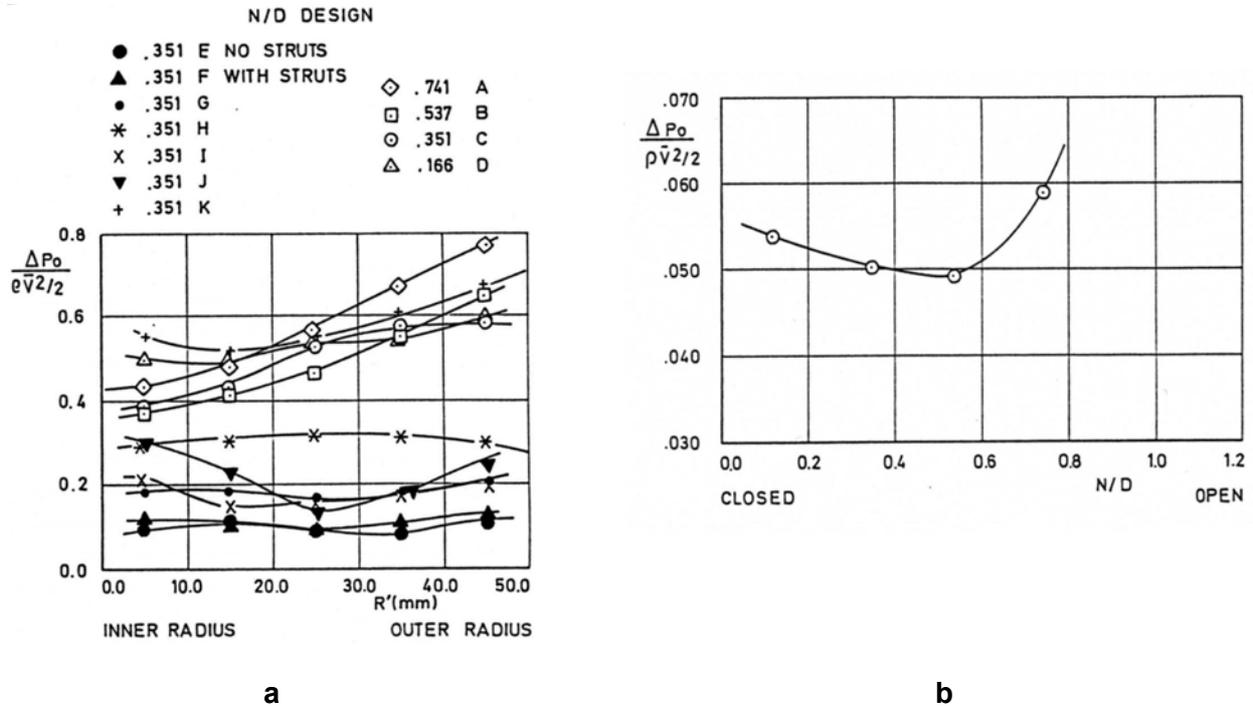
**Figure 11: Radial Variation of Pressure Losses (a)
and Average Losses for Different Geometries (b).**

Further investigations concern the modification of the inlet contour in an attempt to decrease the impact of the inlet geometry on the losses and flow distortion. Results are also summarized in Fig. 11a. Configuration E is without struts. One observes a very large reduction of the losses. Geometry F has small struts that are streamlined and oriented along the flow. This results in equally low losses. One notices in both vanes the strong decrease of overall loss level and a much less distorted flow for both geometries (Fig. 11a).

Test results of five new geometries are describes in [7]. The first two geometries (G,H) use the initial inlet contour as in [6], with respectively 5 or nine circular support struts. Geometry J and K also use 5 or 9 circular support struts but in combination with the modified inlet contour (Fig. 12). Geometry I has 5 large streamlined struts also in combination with the modified inlet contour. The large increase in losses allows estimating how much of the loss decrease in geometry E is due to the removal of the struts and how much loss reduction is the consequence of the contour modification. As expected, the direction of the flow remains unchanged. The losses increase in geometries G and H in comparison to E and F. They have the same overall geometry but less optimally shaped struts. Comparing geometry I with F one observes an increase of losses because of the larger vanes, but the spanwise non-uniformity of the flow decreases.
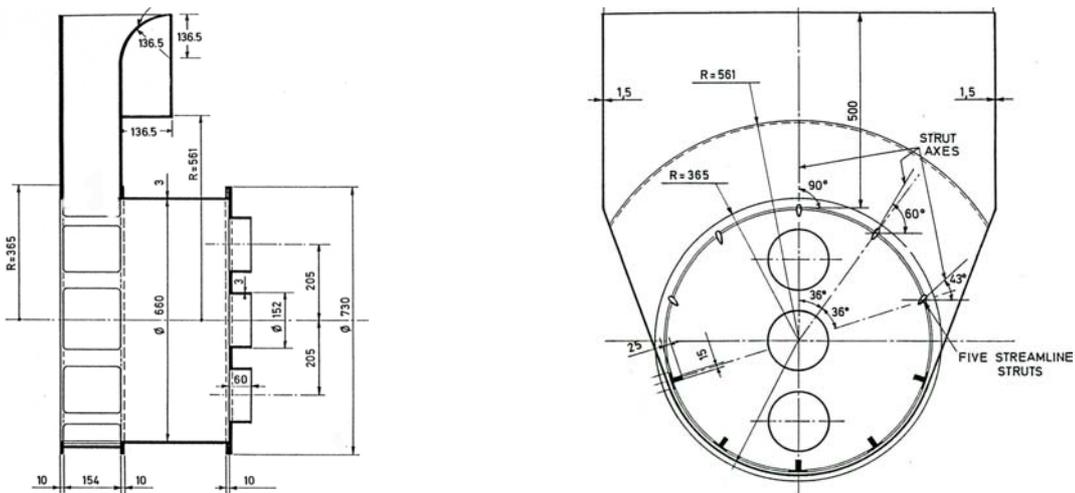
Figure 12: Narrow Inlet Section without Struts (a) or Streamlined Struts (b).

1.5   Vaned Inlet Volutes

A rather expensive way to uniformize the impeller inlet flow is by installing guide vanes in the inlet volute. Flathers et al. [8] present a numerical and experimental study of a vaned inlet. The purpose is to equalize the flow in an accelerating side suction inlet for an industrial centrifugal compressor. A first attempt by installing radial guide vanes, shown on Fig. 13a, was not very successful. The swirl angle survey (Fig.13b) showed a general rotation in the direction of the inflow with local flow angles up to 25.$^{\circ}$. This angle is larger at hub (25% span) than at shroud (99% span). Two counter-rotating vortices can be observed in the bottom dead centre. The static pressure increases from shroud to hub, and from inlet to bottom dead centre. Total pressure losses were highest at shroud, but in general very low.

a

b
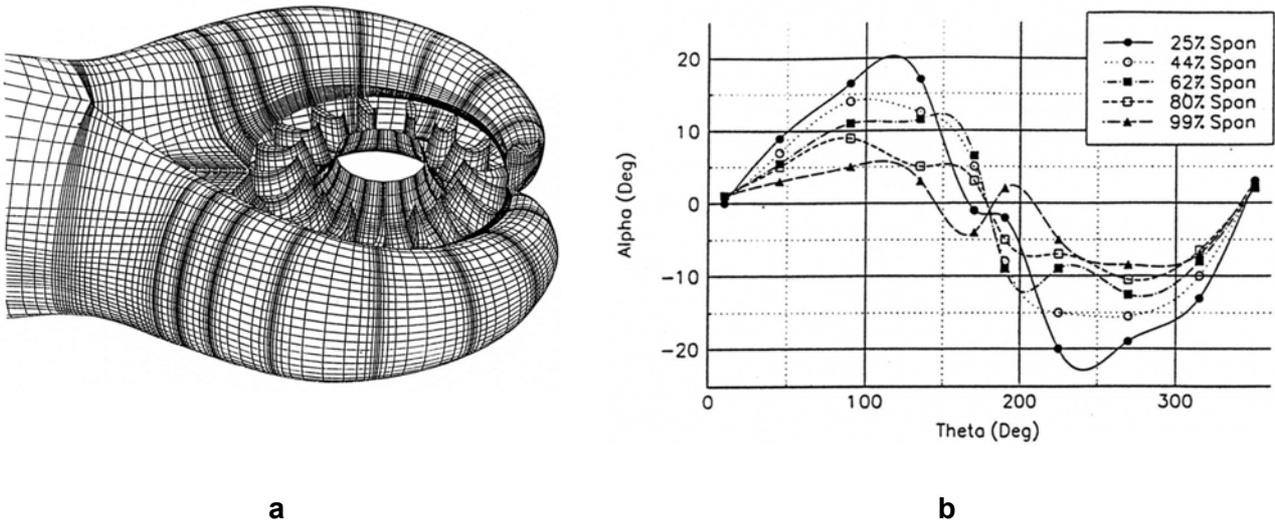
Figure 13: Accelerating Volute with Radial Blades (a) and Resulting Flow Angle Distribution (b).

Cambered guide vanes are proposed to uniformize the flow in the impeller eye. The camber of a baseline vane corrects for the maximum spanwise averaged swirl angle. The leading edge is rounded of in order to allow for a large range in incidence from hub to shroud. The other vanes, used in the model, are less cambered versions of the baseline one, adjusted to compensate for the local measured swirl angle.

Fig. 14a shows a very much equalized flow downstream of the vanes. The swirl angle variations are much lower than for the unvaned case. The static pressure is uniform along the circumference. Total pressure losses are somewhat increased. Both the total pressure and swirl angle distribution show local distortions in the vicinity of the vanes. The blades seem to be the least effective in the shroud region, where one notices the highest losses.

a

b
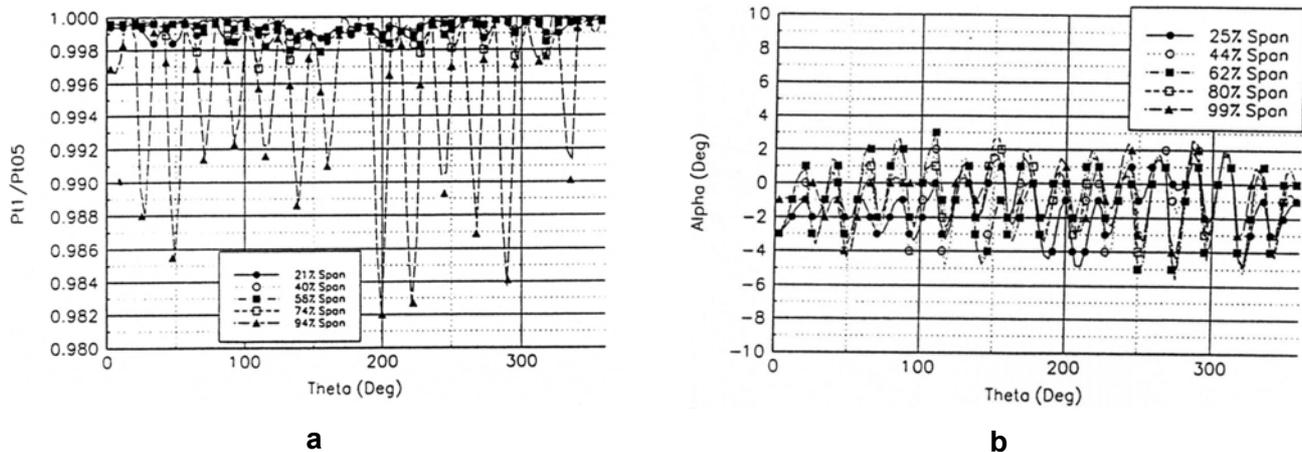
Figure 14: Total Pressure (a) and Flow Angle (b) Variation at Impeller Inlet.

1.6   Conclusions

Total pressure losses are predominant in:

- The top dead centre, where a separation is observed resulting from the sharp turn from radial to axial flow direction.

- At the bottom dead centre, where the flow coming from one side collides with either the flow coming from the other side or with the flow splitter. This collision results in the creation of counter rotating vortices. The flow in this region is influenced by the wake flow of the shaft and the horseshoe vortex coming from the intersection of the shaft with the bottom cover.

- Downstream of the struts or guide vanes.

- At divergent parts of the inlet.

The influence of diffusion can be attributed to the thickening of the incoming boundary layer. As a consequence, the flow is more ready to separate, more sensitive to sharp turns and obstacles in the flow. The flow is also more sensitive to geometrical imperfections. The latter one may possibly lead to an asymmetric flow in an essentially symmetric nozzle.

Flow Angles. The flow in this type of inlets always exhibits a tangential velocity in the direction of inflow. Counter-rotating vortices are observed at the bottom dead centre.

One can only take away the swirl in front of the impeller with well designed guide vanes. These guide vane leading edge should be aligned with the flow and have large leading edge radii to be able to cope with a large variation of incidence angles from hub to shroud. They should be put sufficiently far from, the inlet of the impeller, to allow the mix out of the wakes.

Accelerating flows (in the vicinity of disturbances) not only help to decrease the losses, they also reduce the flow angle distortions because it increases the meridional velocity without influencing the swirl velocity component.

Most of the aforementioned measurements or calculations do not take the presence of the impeller into account. As shown by Tomica et al. [9] the outflow geometry can significantly modify the flow in the nozzle, especially when return flow is occurring.

2. OUTLET VOLUTES

The flow in a suction pipe is mostly parallel and free of swirl with nearly constant total pressure. Only a small amount of vorticity resulting from the boundary layers and secondary flows induced in curves. Hence, potential flow can be an acceptable approximation in many cases. Changing the mass flow (at constant or varying RPM) results in a proportional change in inlet velocity with only small changes of the flow direction. The flow structure is not affected and off design operation is not a big issue. Inlet volutes performing well at design point will also perform well at different mass flows and impeller RPM.

The outlet volutes differ from inlet volutes because the flow can no longer be approximated by a potential one and inlet flow conditions change considerably with both RPM and mass flow. Outlet volutes can be considered as a stator with one vane with a complete circumference as pitch (two vanes at $180.^o$ in case of double volutes). The layout is made for one inlet angle and hence well adapted for only one mass flow per speed line. At off design operation, the volute generates a circumferential variation of the static pressure at the impeller outlet. The main consequence is an unsteady impeller flow with a circumferential variation of mass flow and blade loading.

There is only one mass flow at a given peripheral speed for which the flow enters the stator tangent to the volute suction side. This corresponds to the flow situation "b" on Fig. 15. At higher mass flows (situation "a") the flow enters the stator with negative incidence, resulting into a stagnation point on the suction side and a velocity acceleration (pressure decrease) towards the throat section. At lower mass flow (situation "c") the fluid approaches the tongue with a positive incidence. The flow accelerates around the leading edge suction side (tongue) and the deceleration towards the trailing edge (volute exit) explains the circumferential static pressure rise. Contrarily to inlet volutes the flow structure changes with operating point.
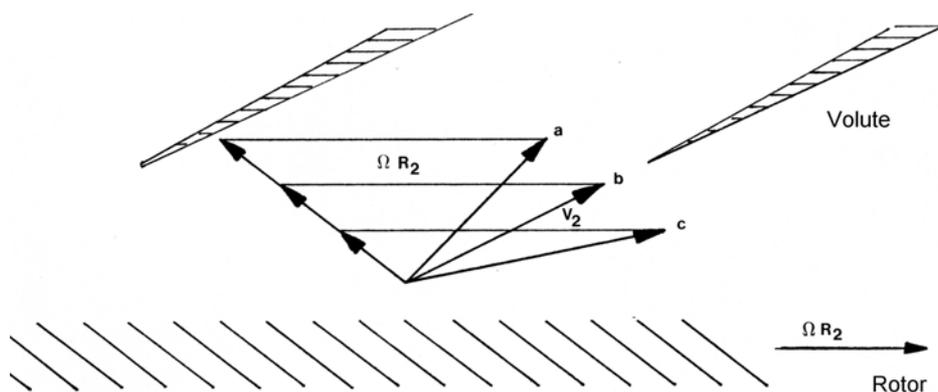
Figure 15: Volute Inlet Flow Conditions at Impeller Off-Design Operation.

The volute circumferential pressure distribution propagates upstream and imposes periodic outlet conditions on the impeller. The impeller exit flow shows a strong variation of the flow angle and total pressure. The potential flow assumption is no longer acceptable.

Another way of looking at the volute impeller interaction, giving also some insight into the loss mechanisms, is illustrated on figure 16. The flow leaving the impeller at lower than optimum mass flow,

has a small radial and a large tangential velocity component. Transporting that small amount of fluid in the volute requires only a small throughflow velocity. This deceleration of the fluid between the impeller exit and the volute cross section, results in a static pressure rise and diffusion losses. The small radial velocity generates a weak swirling motion in the volute. The latter one is dissipated by internal shear and wall friction. It is the second but smaller contribution to the volute losses at low mass flow.
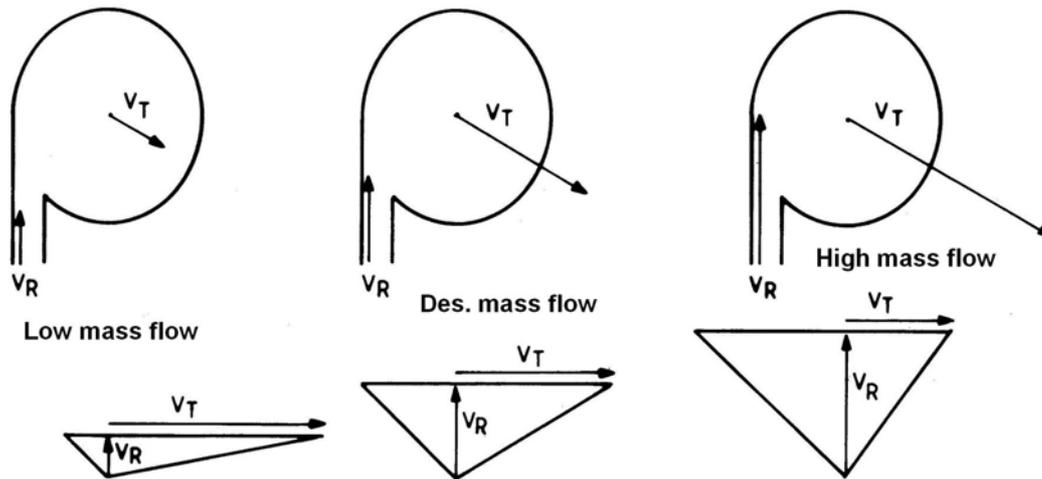
Figure 16: Volute Flow Conditions in Function of Impeller Flow.

The flow leaving the impeller at higher than optimum mass flow has a larger radial and smaller tangential velocity. Transporting that large amount of fluid in the volute requires a larger throughflow velocity than the tangent velocity at the impeller exit. The corresponding acceleration of the fluid results in a static pressure decrease along the volute. This partial destruction of the pressure rise that took place in the impeller and diffuser results in extra losses. The dissipation of the high swirl energy, resulting from the large radial velocity component, is the major source of losses at large mass flow.

At optimum mass flow, the tangential velocity at the impeller outlet relates to the volute through flow velocity by the conservation of tangential momentum. An eventual deceleration defined by conservation of the angular momentum contributes further to the static pressure rise. This is the only way a volute can contribute to the pressure rise without perturbing the circumferentially uniform flow and pressure at the impeller exit. Internal volutes do not profit from this extra flow deceleration and may even result in a pressure decrease and extra friction losses. The swirl generated by the radial impeller outlet velocity is the main source of losses.

2.1   2D Volute Flow

Even in two dimensional volutes with spanwise uniform inlet conditions, the flow will not be uniform over the volute cross sections. Continuity: $\rho . R . V_R = C^{st}$ defines the decrease of the radial velocity component with increasing radius along a streamline in a 2D volute. The tangential velocity changes along a streamline, according to the conservation of angular momentum: $R . V_T = C^{st}$. Combining the two relations results in a logarithmic spiral for the streamlines and outer wall of a 2D volute. A circumferentially uniform V_T distribution at the impeller exit results in a decreasing velocity in the radial direction in section A on Fig. 17 b. Other distributions of inlet tangential velocity, corresponding to lower or higher than optimum mass flows, result in the velocity distributions shown in Fig.17 c (low mass flow) and Fig. 17 d (high mass flow) [10]. The volute flow velocity distribution in a cross section depends as much on the impeller outlet flow as on the volute geometry. Hence, defining the velocity in a cross section by $R . V_T = C^{te}$, is valid only in the design point.
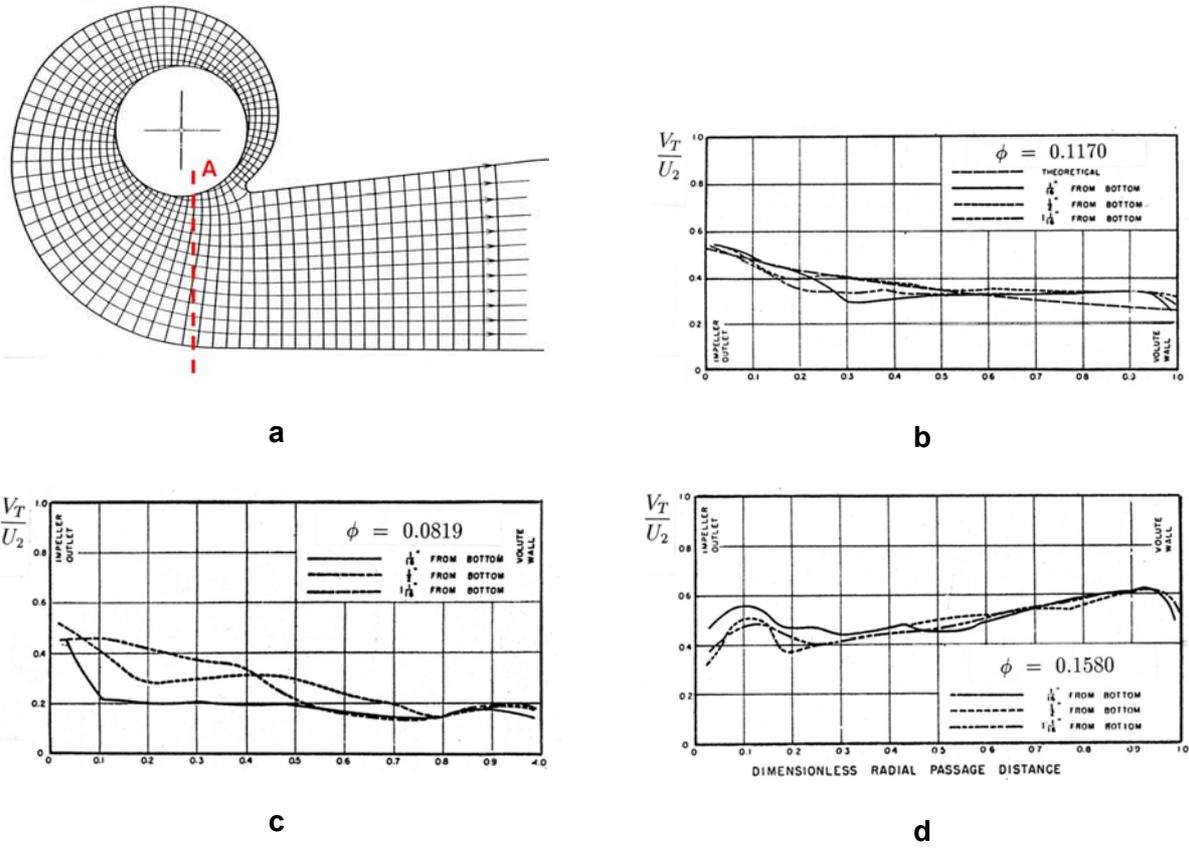
Figure 17: Velocity Distribution in a 2D Volute.

Cross sections can be symmetric or asymmetric, circular, elliptic or rectangular with increasing constant or decreasing radius (Fig. 18). It has been shown [11] that not only the cross section shape but also its radial location has an important influence on the volute losses. Volute cross sections S-1 to S-5 have the same area variation but different radial locations. However, losses almost double with decreasing central radius. Circular cross sections have a small advantage because the smaller wetted surface means smaller friction losses. However one should not conclude that rectangular cross sections result in higher losses because of the flow turning in the 90.° corners. The total velocity has a throughflow component (perpendicular to the cross section) that is often much larger than the swirl velocity component so that the flow approaches the corner tangentially and does not undergo a 90.° turning.
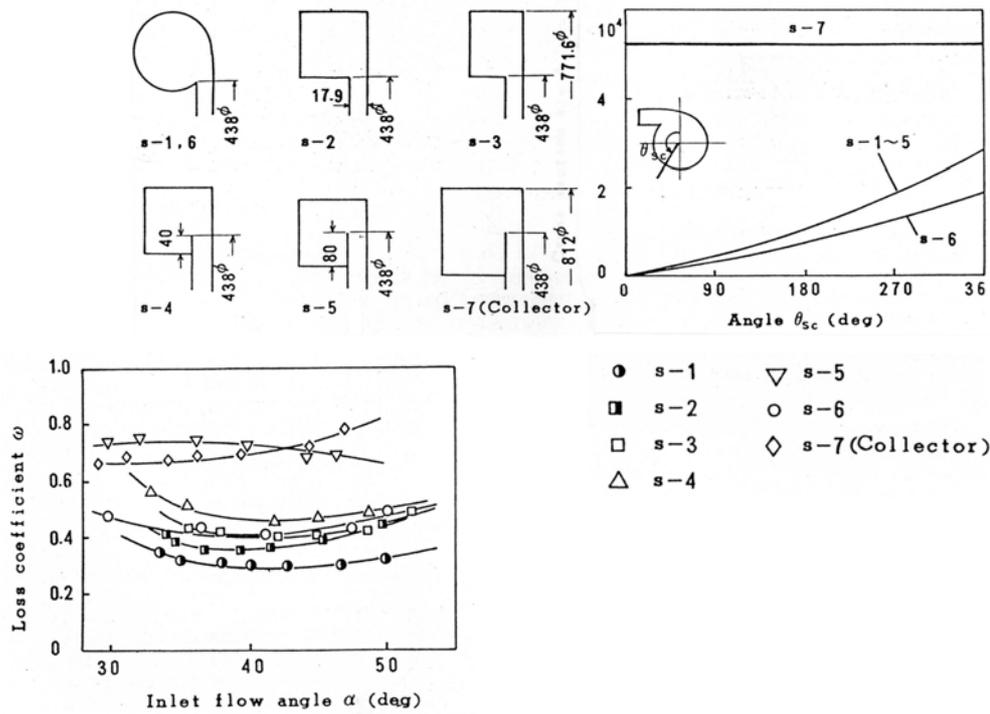
**Figure 18: Volute Losses as a Function of Cross Section and Radial Location.**

The distance between the impeller trailing edge and the volute tongue has an important influence on the circumferential pressure distortion. Larger distances allow for a better smoothing of eventual flow and pressure distortions at the volute tongue in the same way a larger gap between stator and rotor will decrease the interaction. This attenuation is limited as observed by Sideris [12] The remaining circumferential pressure distortion propagates upstream through the vaneless diffuser to the impeller exit. The perturbed velocity field respects the laws of mass- and momentum conservation and the perturbation amplitude may even increase with decreasing radius (fig. 19).
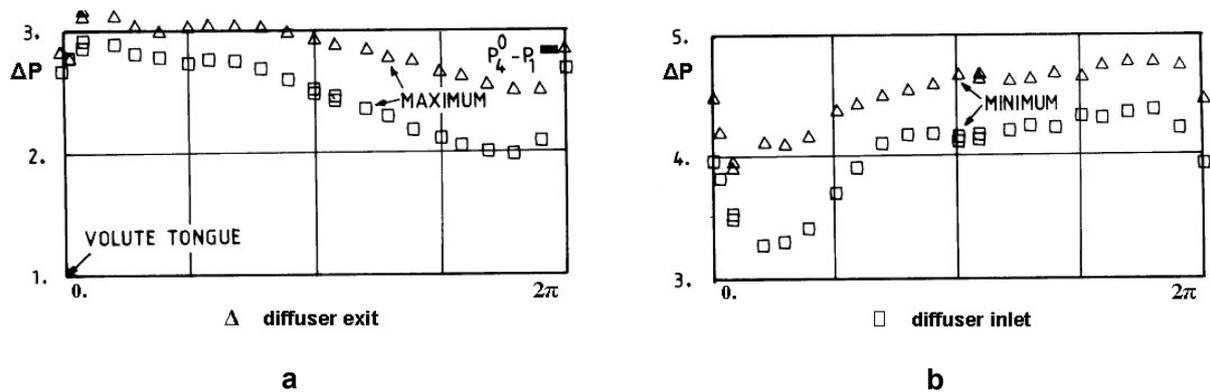

Figure 19: Pressure Variation at a Pump Diffuser Inlet and Exit at Low- (a) and High Mass Flow (b).

2.2   3D Flow in Volutes

The 3D flow in the volute depends on the geometry and on the impeller outlet flow. Even a symmetric volute can show different vortex structures depending on the operating point as shown on Fig. 20 [13].

<center>a   b   c</center>
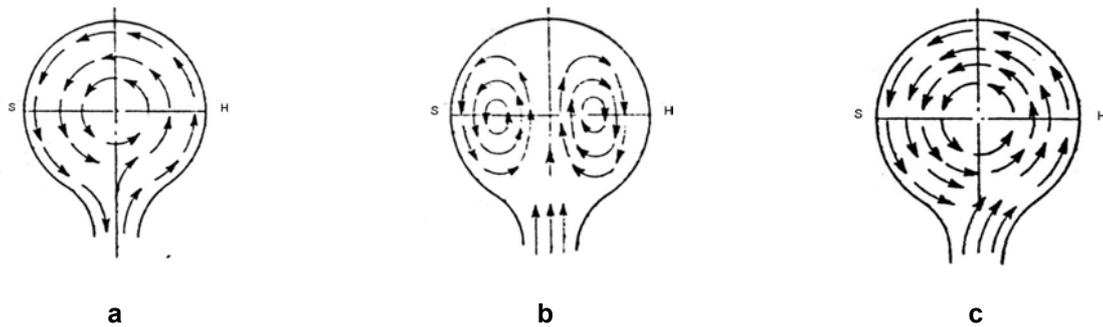
Figure 20: Vortex Structures in a Symmetric Volute at Different Operating Points.

The weak asymmetric vortex observed at zero mass flow (a) may change into two symmetric vortices at design mass flow and back to a strong asymmetric vortex at large mass flow. The last one is the result of a larger radial velocity at the hub side of the impeller exit. The direction of rotation depends on the spanwise variation of inlet conditions. These variations of the flow pattern may lead to discontinuities in the performance curve.

The structure of the vortices depends on the circumferential variation of the inlet flow radial velocity as explained by a linear version of a volute on Fig. 21. The fluid entering close to the tongue, at small radius, fills the centre of the volute. New fluid, entering further downstream at a larger radius, starts rotating around the upstream fluid. Vortex tubes of increasing radius are wrapped around each other and each part of the fluid remains at almost constant radius. Hence the swirl velocity V_S at a given radial position depends on the radial velocity V_R of the fluid at the position where it has entered the volute. The other properties of the flow inside the volute, such as P^o, depend on the incoming flow and on the changes of the vortex structure inside the volute. The circumferentially constant radial velocity at design mass flow theoretically results in a vortex with constant swirl velocity V_S as shown on Fig.22a. However this gives rise to large shear forces in the centre. Kinetic energy is dissipated until a forced vortex structure (friction free solid body rotation) appears in the centre. The shear forces generate losses and are responsible for a decrease of the total pressure in the centre. Radial equilibrium between the swirl velocity and the static pressure creates a zone of low static pressure in the centre defined by:

$$\frac{dP}{dr} = \rho \frac{V_S{}^2}{r} \tag{1}$$
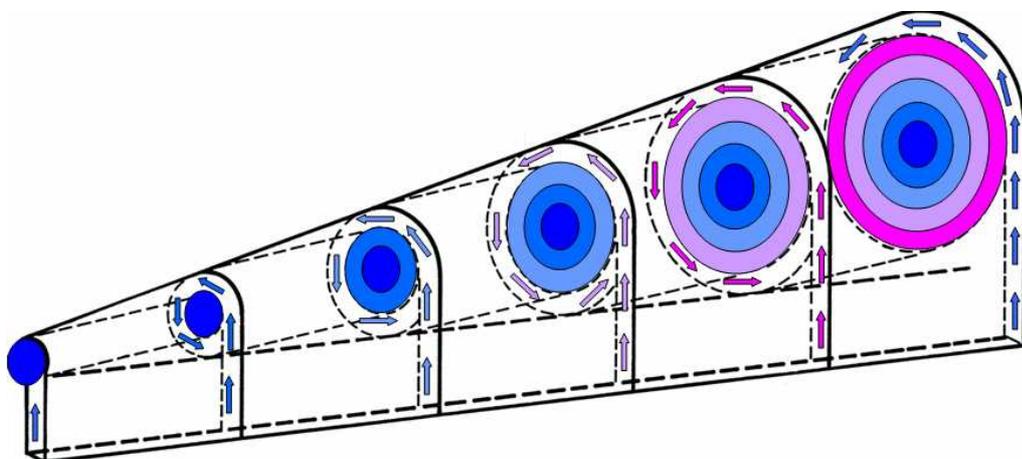
Figure 21: Schematic View on a Straight Volute.

a   **b**
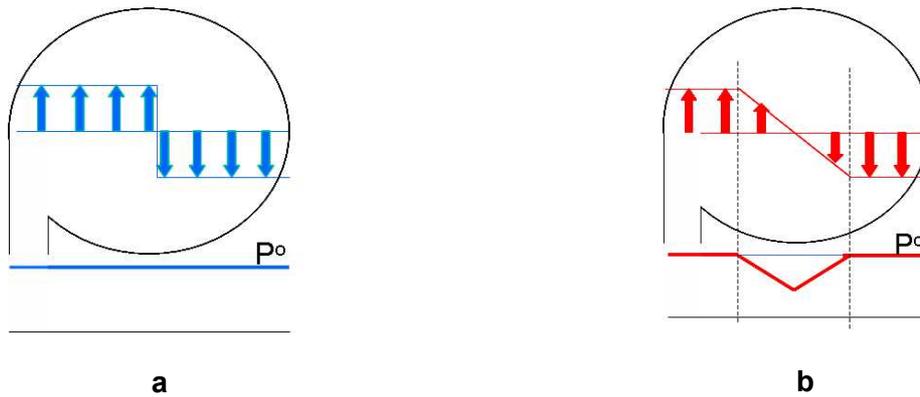
Figure 22: Theoretical (a) and Real (b) Vortex Structure.

The through flow velocity is defined from what is left after the swirl velocity is subtracted from the remaining kinetic energy

$$\rho \frac{V_T^2}{2} = P^o - P - \rho \frac{V_S^2}{2} \tag{2}$$

The velocity and pressure distributions shown on Fig 23 are measured at design mass flow and confirm the model. The swirl distribution shows an almost constant swirl velocity near the walls and a forced vortex type flow in the centre. The large decrease of static pressure towards the centre is a direct consequence of the swirl. The deficit of total pressure in the centre is due to the high shear in the centre of the vortex. The through flow velocity towards the centre is calculated by (2). Its moderate increase towards the centre is a consequence of the small decrease in total pressure in combination with a large decrease of the static pressure and the small swirl velocity in the volute centre.
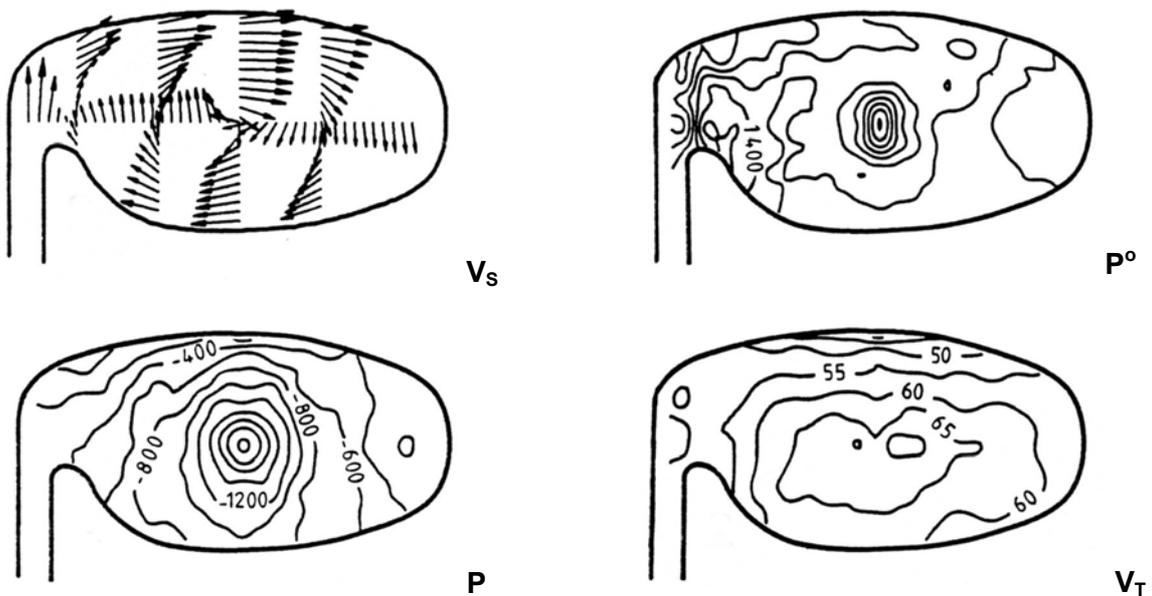
Figure 23: Volute Flow Structure (Design Mass Flow).

At higher than design mass flow, the static pressure at impeller exit decreases from the tongue towards the volute exit. As a consequence the radial velocity is small near the tongue and increases towards the volute exit. According to our model this will result in a forced vortex swirl and the shear stresses and total pressure losses will be minimum. Circumferentially decreasing static pressure results in a decreasing total pressure (less work input) along the impeller exit. Hence the total pressure will be higher in the volute centre than near the walls. Larger mass flow means larger radial velocity at impeller exit and hence results in a larger swirl velocity. The result is a larger decrease of the static pressure towards the centre (eq. 1). The increase of total pressure and decrease of the static pressure in the volute centre results, according to (eq. 2), in a much larger through flow velocity in the centre (100 m/s) than near the walls (65. m/s).
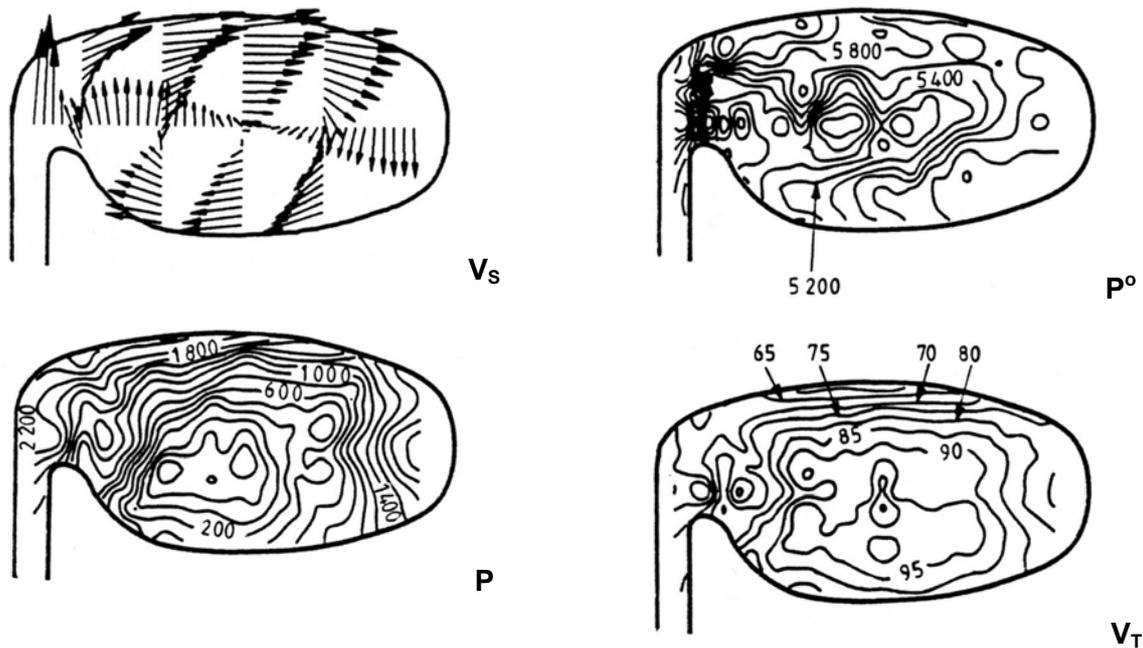

Figure 24: Volute Flow Structure (High Mass Flow).

The opposite occurs at low mass flow. The circumferential increase of static pressure along the volute length results in a decrease of the impeller exit radial velocity and the highest swirl velocity and hence large total pressure losses are generated in the centre of the volute. The weak swirl generates only a small static pressure decease toward the centre so that not much kinetic energy is left. The through flow velocity is decreasing towards the centre. This picture can be observed only if the flow separation, because of too much deceleration of V_T, is not perturbing too much the flow.

The flow model presented here is confirmed by many measurements and calculations at VKI [14, 15, 16]. The increase of through flow velocity in the vortex centre explains why in some cases the optimum cross section area is smaller than the one calculated by a 2D method.

The same system applies to two vortices occurring in symmetric volutes as can be concluded from measurements by Hübl [17] (Fig. 25). The strongest swirl velocity occurs at higher than design mass flow. The change in swirl velocity has only a small impact on the static pressure because the pressure gradient (eq. 1) applies to a smaller distance (vortex radius = .5 volute radius). The increasing total pressure losses in the vortex centres with decreasing mass flow are clearly observed. The nearly constant total pressure at maximum mass flow results in an increase of the through flow velocity in areas where the swirl velocity is low.
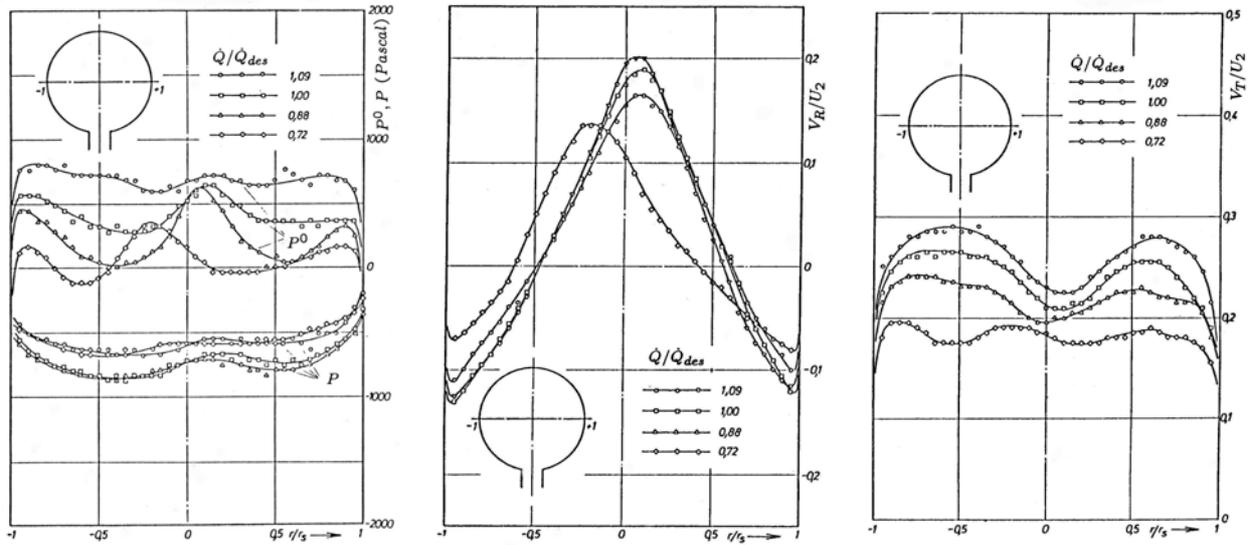
Figure 25: Velocity and Pressure Distributions in a Symmetric Volute.

2.3   1D Volute Loss Models

The overall performance of the volute can be defined by means of a static pressure recovery coefficient

$$C_p = \frac{\overline{P}_4 - \overline{P}_2}{\overline{P}^o{}_2 - \overline{P}_2} \tag{3}$$

and loss coefficient

$$\varpi = \frac{\overline{P}^o{}_2 - \overline{P}^o{}_4}{\overline{P}^o{}_2 - \overline{P}_2} \tag{4}$$

calculated in function of the mass averaged flow quantities at the volute inlet and volute outlet. The ratio of the volute outlet kinetic energy to the inlet kinetic energy is defined by

$$\frac{\overline{P}^o{}_4 - \overline{P}_4}{\overline{P}^o{}_2 - \overline{P}_2} = 1 - (\overline{\varpi} + \overline{C}_p) \tag{5}$$

Values smaller than 1, indicate a deceleration of the fluid between the volute inlet and outlet.

2.3.1   Performance Predictions

One of the prediction models that accounts for the main features of the swirling flow in volutes is the one by Japikse, [18] and extended by Weber and Koronowski, [19]. It assumes that the head, associated with the meridional velocity at the volute inlet, is lost. It is called **meridional velocity dump losses** and expressed by the following equation

$$\Delta P^o{}_{MDVL} = \frac{\rho V_{R2}{}^2}{2} \tag{6}$$

The **friction losses** are calculated in function of a friction coefficient, the hydraulic diameter of the volute channel D_{hyd}, the path length of the fluid particles L within the volute (which is assumed to be equal to the length of the volute channel) and the throughflow velocity V_T inside the volute. Only the throughflow velocity is considered for the friction losses since complete dissipation of the meridional velocity is already accounted for in the meridional velocity dump losses. The friction coefficient ω_F depends on the Reynolds number and surface roughness and can be obtained from the standard friction charts for pipes.

$$\Delta P^o{}_F = \omega_F \frac{L}{D_{hyd}} \frac{\rho V_T{}^2}{2} \tag{7}$$

Two assumptions are made to calculate the **tangential velocity dump losses**:

Firstly, no tangential velocity dump loss occurs if the tangential velocity accelerates from the volute inlet to the volute outlet $V_{T2} < V_{T3}$. However if the tangential velocity decreases from the volute inlet to the exit $V_{T2} > V_{T3}$ then the flow diffuses and it is assumed that the total pressure loss is equivalent to the one of a sudden expansion mixing process.

$$\Delta P^o{}_{TVDL} = \omega_T . \rho \frac{(V_{T2} - V_{T3})^2}{2} \qquad \text{where } \omega_T = 1. \tag{8}$$

Adding the exit cone losses to the volute losses provides a complete prediction model for the losses between volute inlet and pump outlet. The exit cone losses are treated as a gradual expansion and expressed by

$$\Delta P^o{}_{EC} = \omega_{EC} . \rho \frac{(V_{T3} - V_{T4})^2}{2} \tag{9}$$

ω_{EC} depends on the total opening angle of the cone and varies from 0.15 for an opening angle of 10.º to a value of the order 1 for an opening angle of 60.º. Since the opening angle of a well designed volute exit cone should not exceed 10.º, a constant value of 0.15 is proposed by Weber and Koronowski [19].

Japikse shows a good agreement between the calculated and measured variations of $\overline{C}_p$ and $\overline{\omega}$ in function of the volute inlet swirl parameter V_{T2}/V_{R2} and the volute outlet to inlet area ratio (AR) (Fig. 26a and b). Predictions are for similar geometries using dedicated coefficients. It seems that this model provides a useful basis for the prediction of the volute static pressure rise but is much less accurate for the loss prediction. This is surprising because $\overline{C}_p$ and $\overline{\omega}$ are linked by (5). The difference between the calculated and measured values of loss coefficient $\overline{\omega}$ for high mass flows (small values of $V_T/V_{R\,in}$) can be due to neglecting the remaining swirl at the exit of the volute in the model but not in the measurements. For lower mass flows (big values of $V_T/V_{R\,in}$, the influence of the swirl energy is not important and predictions are more accurate.
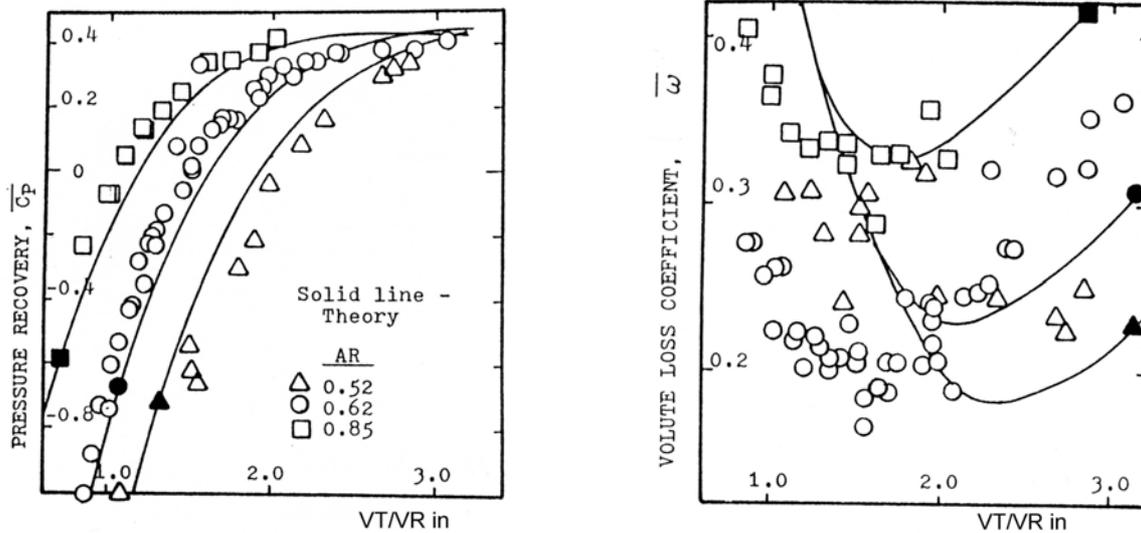
Figure 26: Volute Pressure Recovery and Losses versus Inlet Swirl Parameter.

Experimental and theoretical investigations [19] revealed that the modelling the tangential velocity dump losses, without accounting for the variation of the central radius of the volute, causes an incorrect prediction of the losses especially for the internal type of volutes $R_C < R_{in}$. Weber and Koronowski [19] modified the modelling of the tangential velocity dump losses. This provides some improvements but there are still a large number of cases with a rather poor agreement.

The model of Iverson [20] may give correct predictions for symmetric volutes with negligible swirl. More complex geometries however require more complete models. In view of previous experimental data, there is no interest in verifying volute prediction models that neglect the swirl over the volute cross section [20]. Also the assumptions of uniform inlet and outlet flow conditions may not be satisfied.

2.3.2 Detailed Evaluation

The assumption of circumferential uniform flow is not correct and may be the main limit of applicability of the 1D method. The detailed experimental data of the elliptic volute presented in [15] and [16], of which some results are shown in Fig. 23 and 24, have been used to evaluate previous model and to find out the possible sources of discrepancies between experiments and predictions. Results are summarized in table 2.

Table 2: Measured versus Calculated Total Pressure Losses (Pa)

	High mass flow			Medium mass flow			Low mass flow		
	Calculated		Meas.	Calculated		Meas.	Calculated		Meas.
	1D	DATA	Meas.	1D	DATA	Meas.	1D	DATA	Meas.
$\Delta P^{o}{}_{F}$	2483			982			281		
$\Delta P^{o}{}_{MVDL}$	1453	2486	1939	492	791	674	94	157.5	126
$\Delta P^{o}{}_{TVDL}$	98			9			215		
Ω_{T}	.2			.2			.5		
$\Delta P^{o}{}_{in\text{-}out}$	4034	5067	4520	1478	1777	1660	590	653	622
$\Delta P^{o}{}_{MC}$			547			117			31
$\Delta P^{o}{}_{EC}$	2414	1381	1381	696	397	397	89	26	26
Q_{out}-Q_{exit}	2230	2230	5654	754	754	1517	145	145	329
ω_{EC}	1.1	.62	.24	.92	.53	.26	.61	.18	.08
$\Delta P^{o}{}_{TO}$	6448	6448	4848	2174	2174	2174	679	679	679
C_{pEC}			.578			.483			.55

The losses shown in the first column are the ones calculated as functions of the velocity components predicted by a one dimensional analysis model, assuming uniform flow at the inlet and outlet sections. The results in the second column are calculated as functions of the real velocities and pressures obtained by mass averaging the detailed experimental data. The average velocity at the volute outlet is evidently the same as in the one dimensional model. The mass averaged pressure and kinetic energy, however, is different from the ones calculated by the one dimensional model. The third column contains the measured values.

The non-uniformity of the radial velocity at the volute inlet results in a higher swirl at off design operation than the one calculated with a uniform velocity. The corresponding meridional dump losses (column 2) are therefore higher than the ones predicted by the one dimensional model (column 1). The real volute swirl losses (column 3), however, are lower by the amount of residual swirl measured at the volute exit.

The volute total pressure losses obtained by comparing the mass averaged $P^{o}{}_{out}$ and $P^{o}{}_{in}$ (column 3) can be used to quantify the friction- and tangential flow losses. The loss coefficients for tangential flow loss under accelerating and decelerating flow conditions in the volute can be determined by requiring consistency of the friction loss model, i.e. a constant friction loss coefficient under all three flow conditions. The average Reynolds number at the operating conditions of the tests is approximately 3.10^{5}. For this Reynolds number the pipe friction coefficient depends mainly on the relative surface roughness. For the investigated volute the relative surface roughness $\varepsilon / D_{hyd} = .001$, and results in a ω_{F} value of 0.019.

Friction losses calculated as a function of the average throughflow velocity in the volute and mean hydraulic diameter are given by $\Delta P^{o}{}_{F}$ in Table 2. They are the same for the 3 different ways of calculating the losses. The remaining tangential velocity dump losses can now be calculated by elimination. Since at medium mass flow the volute inlet velocity is almost equal to the volute outlet velocity, no tangential flow losses should occur. This is in agreement with the very low value of $\Delta P^{o}{}_{TVDL}$ at medium mass flow.

In case of decelerating flows (low mass flow) the resulting tangential velocity dump losses are well predicted by a coefficient $\omega_{T} = .5$. This is the same value as the one proposed in previous investigations [18,19]. A value of $\omega_{T} = .2$ is required in (eq. 8) for accelerating flows. This value is lower than for decelerating flows as can be expected.

Exit cone losses are obtained by subtracting the volute losses from the total losses. Different values are obtained depending on the volute losses. The real exit cone losses are the sum of the cone diffusion losses $\Delta P^o{}_{EC}$ and the remaining swirl losses $\Delta P^o{}_{MC}$. The loss prediction (eq. 9) concerns only the exit cone diffusion losses. Taking into account the non uniformity of the meridional velocity, the measured inlet kinetic energy results in the ω_{EC} coefficient shown in column 3. This value is larger at high and medium mass flow, as can be expected from the non uniformity of the inlet flow. In spite of the high losses at high and medium mass flow, relatively large values of the static pressure rise coefficient $C_{p_{EC}}$ are observed.

This is due to the stabilizing effect of the swirling flow on the exit cone diffuser [18].

Very high loss coefficients (column 1) are needed to predict the exit cone losses by the one dimensional model. This results from an overestimation of the cone losses (because of an underestimation of the volute losses), and an underestimation of the inlet dynamic pressure, by the one dimensional model, neglecting the inlet non-uniformity at high and medium mass flow.

Calculating the real exit cone losses as function of the inlet dynamic pressure, predicted by the one dimensional model, requires a loss coefficient between 0.18 and 0.62 (column 2). These values are close to the conventional values. A variation of the loss coefficient ω_{EC} is required to account for the inlet distortion, whatever model is used to calculate the exit cone losses.

2.4   2D Volute Loss Model

The main shortcomings of previous volute prediction models result from the lack of knowledge of the real velocity distribution at the different cross sections. Inlet velocity, swirl velocity and throughflow velocity may be very non uniform. This makes the kinetic energy, available at each cross section, very different from the one evaluated with the uniform flow assumptions. A second limitation is the inability of the 1D model to predict the circumferential pressure distortion resulting from the volute off-design operation. Such a calculation would considerably improve the prediction of the impeller performance. However, it requires a model for the impeller response to an outlet distortion in order to predict the non uniform volute inlet velocity in function of the pressure distortion. More complete models, taking into account the circumferential pressure distortion and cross-wise non-uniformity of the flow, have been presented by Hübl [17]; Van den Braembussche [21]. One could call them 2D models because they account for the circumferential variation of the volute inlet flow and the axisymmetric variation of the flow over the volute cross section.

The flow inside a volute and the resulting circumferential static pressure distortion and total pressure losses are calculated by an iterative procedure to account for the volute-impeller interaction. Imposed is, the static pressure at the impeller exit and the non uniform flow (velocity and angle) at the volute inlet. The method consists of the following modules:

The **impeller response calculation** defines the circumferential velocity distribution V_{R2} and V_{T2n} resulting from a circumferential variation of the outlet static pressure distribution. One uses a model evaluated by Sideris et al. [12]. It is based on the impeller response model presented [22] and [23]. It relates the local change of mass flow (radial velocity component) to the difference between the local pressure rise and the one corresponding to the velocity triangles.

$$\frac{\partial V_{R2}}{\partial t} = -U_2 \frac{\partial V_{R2}}{R_2 . \partial \theta} + \frac{\cos \beta_{bl}}{EL}(U_2 V_{T2} - U_1 V_{T1} + \frac{P^o{}_1 - P_2(\theta)}{\rho} - \frac{V^2{}_{R2} + V^2{}_{T2}}{2}) \tag{10}$$

where EL is the equivalent length of the impeller flow channel. The radial velocity distribution can be obtained by a numerical integration in time using an explicit one step Lax-Wendroff discretization scheme. Sideris [12] showed that the best results are obtained by assuming no circumferential variation of

V_{T2}. At the first iteration, the static pressure is assumed to be constant and the volute inlet velocity is defined by the circumferentially-averaged value.

The **volute flow calculation** approximates the three-dimensional flow in the volute. Starting from the non-uniform impeller outlet flow, the module defines the volute losses and static pressure rise, and updates the circumferential static pressure distortion at the volute inlet. Shown on Fig. 27 is an approximation of the model explained in section 2.2. The isentropic local swirl velocity V_S and total pressure is related to the inlet flow radial velocity and inlet total pressure distribution by continuity considerations. The difference between the calculated swirl distribution and the real forced vortex swirl distribution provides the local pressure losses in the volute centre. The crosswise static pressure distribution is obtained from the radial equilibrium (eq. 1) and the crosswise trough flow velocity V_T is defined by (eq. 2). The procedure is iterative because a change in V_T over the cross section influences the continuity considerations as illustrated on Fig. 27.
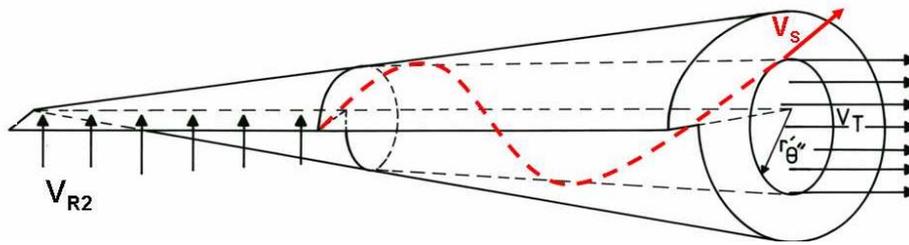

Figure 27: Volute Flow 2D Prediction Model.

The **Volute pressure calculation** predicts the impeller outlet circumferential static pressure distortion as a function of the volute circumferential pressure variation. Applying the tangential momentum equation on discrete control volumes of the volute allows the calculation of the static pressure at the exit of each volute element (θ_o) in function of the flow parameters at the inlet section (θ_i), outer wall (*ow*) and inner wall (*iw*) Fig. 28.

$$\rho_2 V_{R2} 2\pi R_2{}^2 b_2 V_{T2} + R_C(\theta_i) A(\theta_i)\left(P(\theta_i) + \rho(\theta_i) V^2{}_T(\theta_i)\right) + dA_{iw}\left(\overline{P} - \overline{\rho}\overline{V}^2{}_T \frac{\overline{R}_C - R_{Ciw}}{R_{Ciw}}\right) R_{Ciw} +$$

$$dA_{ow}\left(\overline{P} - \overline{\rho}\overline{V}^2{}_T \frac{\overline{R}_C - R_{Cow}}{R_{Cow}}\right) R_{Cow} = R_C(\theta_o) A(\theta_o)\left(P(\theta_o) + r(\theta_o) V^2{}_T(\theta_o)\right)$$

(11)
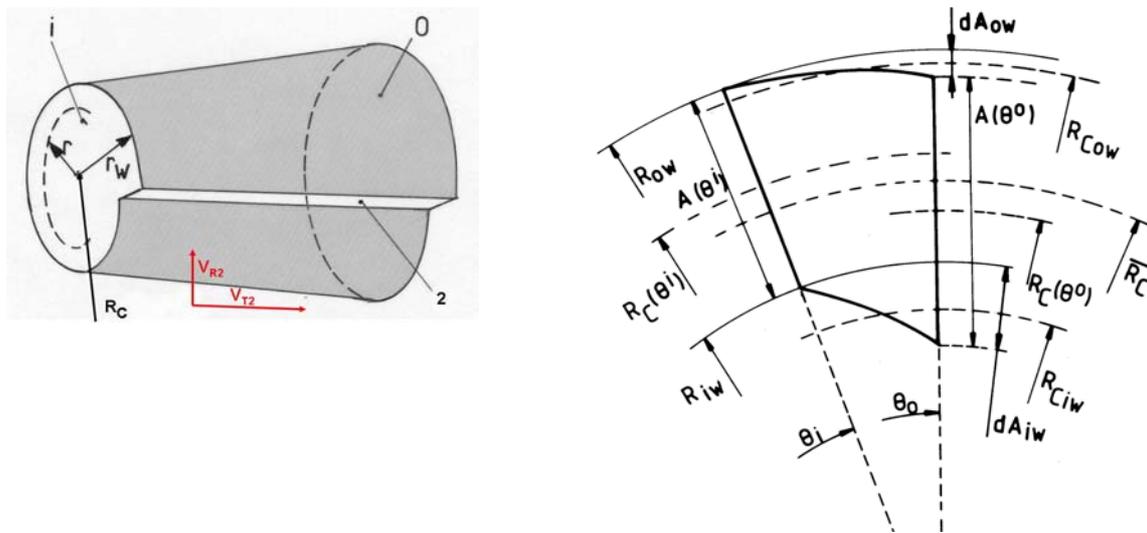
Figure 28: Discrete Volute Control Volume.

This calculation makes use of the average flow conditions calculated at the mean radial position of each surface and cross section. This volute inlet pressure, together with the volute losses and static pressure rise coefficient are the main results of the volute calculation.

The **Exit diffuser flow calculation** is the same as for the 1D model.

Each of these components are explained in more detail in [21]. With the exception of the last one, used only once for the overall performance calculations, these components are combined in an iterative procedure in which the flow conditions at impeller outlet are adjusted. The static pressure distortion, resulting from the volute calculations, is imposed at the impeller exit where it is an input for the impeller response model. The latter one provides the circumferential variation of the total pressure and tangential and radial velocity at the volute inlet. The iterative procedure is stopped when the new impeller outlet pressure distribution equals the previous one.

Fig. 29 shows a comparison between the measured and calculated static pressure rise- and total pressure loss coefficients. One observes a good agreement except at minimum mass flow, where larger losses and lower static pressure rise are due to flow separation in the volute exit cone diffuser. The method is equally applicable to volutes with rectangular cross sections. In those cases the rectangular cross section is replaced by an elliptical one with the same cross section area and height over width ratio. Although the method requires an non negligible amount of input (geometry) its main advantage is its completeness (inclusive rotor response model) and much shorter calculation time than a 3D Navier Stokes calculations.
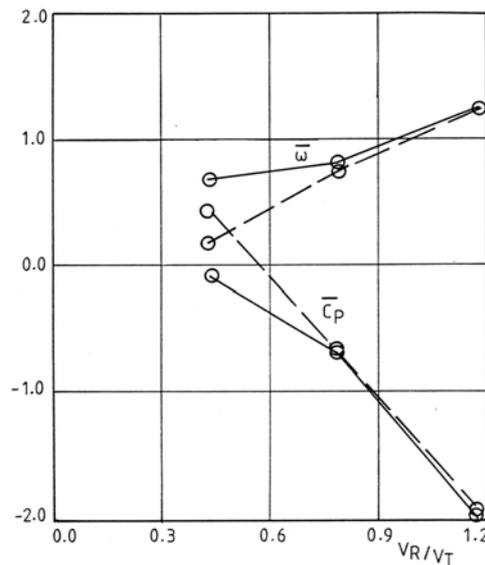
Figure 29: Comparison between Experimental and 2D Prediction Results.

2.5   Conclusions

The volute flow is equally dependent on the geometry as on the impeller exit flow conditions. The later one depends on the volute circumferential pressure distortion. This means that ny prediction method should account for this strong interaction.

Swirl is the main source of losses in a volute. Optimum volute performance requires minimum radial velocity at impeller exit. Simultaneous optimization of the impeller and the volute is recommended.

BIBLIOGRAPHY

[1]   Matthias, H.B.: The design of pump suction bends, IAHR-Symp. Braunschweig, VDI-Verlag 1966, S. E 21-30.

[2]   Pinckney, S.: Optimized turning-vane design for an intake elbow of an axial-flow compressor. NASA Report TN D-3083, 1965.

[3]   Kovats, A.: Effect of non rotating passages on performance of centrifugal pumps and subsonic compressors. Flow in primary non-rotating passages in turbomachines, ASME, 1979.

[4]   Lüdtke, K.: Centrifugal process compressors - radial vs. tangential suction nozzles. ASME Paper 85-GT-80, 1985.

[5]   Neumann, B.: the interaction between geometry and performance of a centrifugal pump. Mechanical Engineering Publications Ltd., London.

[6]   Ligrani, P., Breugelmans, F.: The influence of inlet geometry characteristics on flow uniformity in a compressor, von Karman Institute Report, 1979.

[7]   Ligrani, P., Camci, C., Breugelmans, F.: The effect of support strut geometry on flow uniformity in a compressor scale model, von Karman Institute Report, 1980.

[8]   Flathers, M., Bache, G., Rainsberger, R.: An experimental and computational investigation of flow in a radial inlet of an industrial pipeline centrifugal compressor. ASME Journal of Turbomachinery, Vol. 118, No 2, 1996, pp. 371-377.

[9]   Tomica, H., Wonsak, G., Saxena, S.: Ausbildung und Untersuchung von Saugkrümmern für zweiflutige, radial angeströmte Kreiselpumpen, Karlsruhe. Pumpentagung, 1973.

[10]   Bowerman R.D.& Acosta A.J.: Effect of the volute on performance of a centrifugal pump impeller. ASME transactions, Vol. 79, 1957, pp. 1057-1069.

[11]   Mishina, H., Gyobu, I.: "Performance Investigations of Large Capacity Centrifugal Compressors", ASME paper 78-GT-3.

[12]   Sideris, M., Van den Braembussche, R.A.: "Influence of the Circumferential Exit Pressure Distortion on the Flow in an Impeller and Diffuser", Trans. ASME, Journal of Turbomachinery, Vol 109, No. 1, January 1987, pp. 48-54.

[13]   Peck, J.F.: Investigations concerning flow conditions in a centrifugal pump and the effect of blade loading on head slip, Proc. IME, 1951, Vol. 164, pp. 1-30.

[14]   Ayder, E., Van den Braembussche, R.A.: "Experimental Study of the Swirling Flow in the Internal Volute of a Centrifugal Compressor", ASME Paper 91-GT-7.

[15]   Ayder, E., Van den Braembussche, R.A.: "Experimental and Theoretical Analysis of the Flow in a Centrifugal Compressor Volute", Trans. ASME, Journal of Turbomachinery, Vol 115, No. 3, July 1993, pp. 582-589.

[16]   Ayder, E., Van den Braembussche, R.A.: "Numerical Analysis of the Three-Dimensional Swirling Flow in Centrifugal Compressor Volutes", Trans. ASME, Journal of Turbomachinery, Vol. 116, Nr. 3, July 1994, pp. 462-468.

[17]   Hübl, H.P.: "Beitrag zur Berechnung des Spiralgehäuses von Radialverdichtern u. Vorherbestimmung seines Betriebsverhaltens", Technische Universität Wien, Nr. 7, (1975).

[18]   Japikse, D.: "Advanced diffusion levels in turbocharger compressors and component matching", Proc. First Int. Conf. on Turbocharging and Turbochargers, London IMechE., 1982, pp. 143-155.

[19]   Weber, C.R., Koronowski, M.E.: "Meanline Performance Prediction of Volutes in Centrifugal Compressors", ASME paper 86-GT-216.

[20]   Iversen, H., Rolling, R., Carlson, J.: "Volute Pressure Distribution, Radial Force on the Impeller and Volute Mixing Losses of a Radial Flow Centrifugal Pump", Trans. ASME, Journal Engineering for Power, Vol. 82, No. 2, April 1960, pp. 136-144.

[21]   Van den Braembussche, R.A., Ayder, E., Hagelstein, D., Rautenberg, M.: Improved model for the design and Analysis of Centrifugal Compressor Volutes, Trans. ASME, Journal of Turbomachinery, Vol. 121, No. 1, 1999.

[22]   Lorett, J.A. and Gopalakrishnan, S.: Interaction Between Impeller and Volute of Pumps at Off Design Conditions, Trans. ASME, Journal of Fluids Engineering, Vol. 108, No 1, 1986, pp. 12-18.

[23]   Frigne, P. and Van den Braembussche, R.A.: A theoretical model for Rotating Stall in the vaneless Diffuser of a Centrifugal Compressor. Trans. ASME, Journal of Engineering for Gas Turbines and Power, Vol. 107, pp. 507-513.